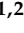*Article*

Shot-Earth as Sustainable Construction Material: Chemical Aspects and Physical Performance

Luisa Barbieri [1,2] , Luca Lanzoni [1,2] , Roberta Marchetti [1], Simone Iotti [3] , Angelo Marcello Tarantino [1,2] and Isabella Lancellotti [1,2,*]

1 DIEF—Department of Engineering "Enzo Ferrari", University of Modena and Reggio Emilia, 41125 Modena, Italy; luisa.barbieri@unimore.it (L.B.); luca.lanzoni@unimore.it (L.L.); roberta.marr@gmail.com (R.M.); angelomarcello.tarantino@unimore.it (A.M.T.)
2 CRICT-UNIMORE: Inter-Departmental Research and Innovation Centre on Construction and Environmental Services, University of Modena and Reggio Emilia, 41125 Modena, Italy
3 HEIG-VD/HES-SO—Haute Ecole d'Ingénierie et de Gestion du Canton de Vaud, Route de Cheseaux 1, CH-1401 Yverdon, Switzerland; simone.iotti@unimore.it
* Correspondence: isabella.lancellotti@unimore.it

Abstract: Soil has long been one of the most widely used building materials globally. The evolution of soil-based construction materials has seen steady improvement over the centuries, even as traditional materials have given way to newer options like reinforced concrete. Nonetheless, soil-based construction has maintained its relevance and, in recent decades, has garnered increased attention due to sustainability concerns and renewed research interest. Among the innovative earth-based materials, shot-earth (SE) stands out as one of the most advanced. Research on SE has facilitated efficient handling of soil variability in mix design and provided structural engineers with relevant models for dimensioning and detailing reinforced SE constructions. This paper focuses on studying the durability characteristics of various types of SE to ascertain their ability to withstand environmental degradation over their intended lifespan. The tests conducted indicate that SE can serve as a viable construction material in numerous real-life scenarios, offering a sustainable alternative to existing materials.

Keywords: shot-earth; physical properties; chemical composition; water absorption; durability

1. Introduction

Construction materials made from excavated soil are considered sustainable because they have a positive impact on the construction industry's supply chain and help reduce its environmental impacts. Given that soil constitutes the most abundant construction waste, with an annual amount of 18 million tons of unpolluted soil excavated in Switzerland [1], it becomes evident that the positive effects on the environment and society also include a reduction in landfill waste and the associated logistical costs and impacts [2]. Moreover, a more efficient yet lighter supply chain, reduced landfilling of waste, and decreased construction material costs, all contribute to cost reduction, thereby creating opportunities to enhance the financial sustainability of construction projects.

Switzerland has heavily invested in cleantech innovation in recent decades, leading to the emergence of numerous innovations in soil-based construction materials [3]. Similarly, other countries have also made significant investments in the development of cleaner materials, including those based on soil [2,4,5]. However, a further step must be taken to reach a stage where these innovations penetrate the construction materials market. The rationale is simple: despite the merits of these sustainable materials, professionals such as architects, engineers, developers, authorities, and contractors need to be confident that these materials can be used without compromising the safety, serviceability, and durability

of constructions. Additionally, they must ensure that these materials can be manufactured and installed seamlessly while remaining economically viable.

Shot-earth (SE) is a new construction material [6] that has been developed in close collaboration with the construction industry. Aspects like the design models that apply to reinforced SE structures [7], creep behavior, mix design techniques, and models to predict the strength that will be obtained using a particular excavation soil [3] have been researched. Therefore, SE is one of the closest candidates to reach the market. Despite this major advancement, the construction business in punctuated by different use cases that require particular aspects to be researched (see Figure 1). One of these is the capacity of the material to withstand over time the different environmental conditions of the site where a specific structure will be built. In order to be able to predict the performances over time under a specific environmental aggression, the material must be holistically understood.

Figure 1. A wine cellar in Biel/Bienne, Switzerland: its walls are constructed using SE, capable of accommodating 400 bottles. These walls, along with the vault and pavement made of excavation earth rasillas, ensure perfect storage conditions for the wine (www.pittet-artisans.ch, accessed on 12 January 2020 [8]).

The durability of soil-based materials has been the subject of intense but sparse research, resulting in several knowledge gaps in both testing methods for their durability and the mineralogy of these hardened materials. This knowledge is essential for accurately assessing the durability properties of materials such as SE, optimizing the mixed design process, and preparing predictive models for scenario analyses. Several studies about the durability of conventional cement-based composites can be found in the literature. As an example, carbonation, shrinkage, creep, and water absorption of low-cement concretes is addressed in [9]. An optimization analysis of the mix of low-cement concretes to improve durability is provided in [10]. The consequences of the crystallization pressure during the hydration of Portland reaching the ultimate tensile strength of concrete matrix, thus getting worse durability, is discussed in [11]. The effects of introduction of additives as recycled granite quarry dust or nanosilica particles on physical performances of cementitious mortars is discussed in [12,13], respectively.

This paper reports a series of studies conducted on the chemical and physical characteristics of two particular mixes of SE [14,15], aiming to fill a gap in the understanding of the durability of soil-based materials and to compare the durability and mineralogical characterization of SE with standard cementitious materials.

Specifically, a wide experimental campaign was devoted to identifying and quantifying the main chemical and physical properties of SE, with specific reference to density, porosity, water absorption [9–11], and resistance to specific aggressive agents such as HCl, HNO_3, and H_2SO_4 [11–13]. As confirmation of the extrapolated data, a XRD spectra analysis post acid attacks was conducted, enabling the identification of primary phases

susceptible to chemical degradation within the SE, contrasting it with conventional cementitious composites.

This has underscored the comparable, and sometimes even superior, durability of SE compared to mortar and ordinary concrete, highlighting its innovative potential for further application in the construction field.

2. Materials and Methods

SE is fabricated and cast using a modified shotcrete dry process [2,6]. The process accelerates a mixture of excavated earth, coarse aggregate, and, if needed, stabilization, through a nozzle at a speed reaching 300 km/h (Figure 2a–c). Water is added at the nozzle in small percentages. The process guarantees optimal compaction and green strength. For stabilization, a binder like gypsum, hydraulic lime, cement, or others can be used, depending on the application. For some applications, no stabilization is needed. Aggregates can be reclaimed from sieving the excavation soil or from deconstruction wastes.
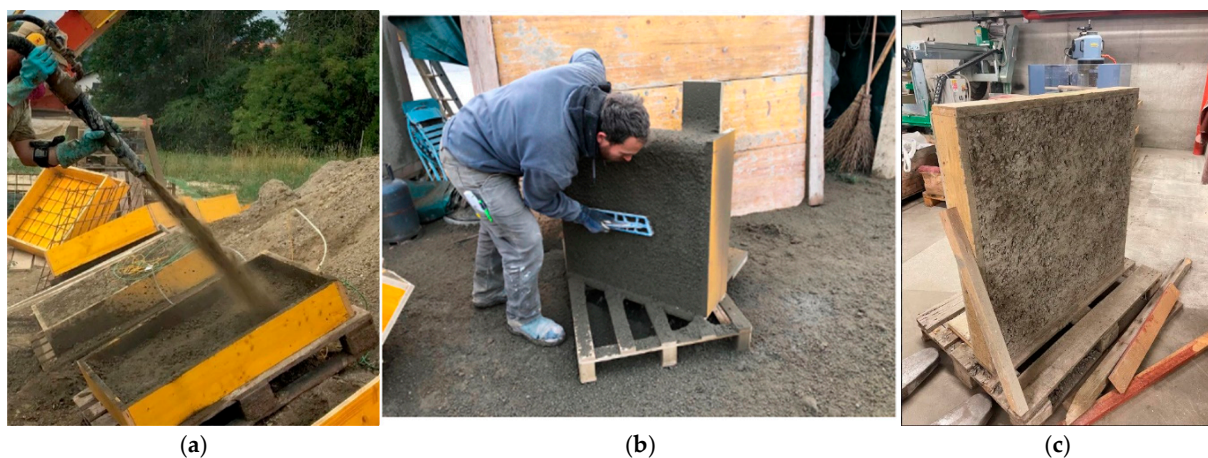

(a) (b) (c)

Figure 2. (**a**) 45° manufacturing method, (**b**) final refinement to smooth exposed surface; (**c**) SE panel after curing [6].

In this study a SE 772 was used, and the numbers indicate the parts in volume of the excavation earth, the aggregate, and the stabilization. Prismatic samples made of SE were realized and compared in terms of compressive strength (M) with two different types of construction materials: concrete from core drilling (C) and a mortar with Portland cement classified as M20. The mixes of the concrete and the cementitious mortar are shown in Tables 1 and 2, respectively.

Table 1. Mix design of the concrete.

Cement	Aggregates				W/C
	Dosage	0–3 mm	3–5 mm	5–10 mm	10–25 mm	
CEM II/A-L 32.5 R	340 (kg/m^3)	935 (kg/m^3)	65 (kg/m^3)	400 (kg/m^3)	565 (kg/m^3)	0.52

Table 2. Mix design of the cementitious mortar.

Cement	Dosage	Sand	W/C
CEM II 32.5 R	1 part	3 parts	0.5

Mixes outlined in Tables 1 and 2 have been adopted to obtain a plain concrete and standard cementitious mortar without additives, thus exhibiting standard performances. This allows comparing the SE performances with those of commonplace building materials.

2.1. True Density, Bulk Density and Porosity

In order to quantify the main physical characteristics of the samples, true density, D_{true}, was measured by a helium pycnometer (Micrometrics Accupyc 1340, Norcross, GA, USA) using a sample in the form of a little piece with variable dimensions according to UNI EN 1936:2006 [16] regulation. Bulk density, D_{bulk}, was geometrically evaluated as the ratio between the measured mass and the known volume. Therefore, porosity *P* was evaluated through Equation (1):

$$P = (1 - D_{bulk}/D_{true}) \times 100 \tag{1}$$

2.2. Capillary Water Absorption

Capillary absorption test was performed following the UNI-EN 1015-18:2004 [17] by applying an impermeable sealant on the sides of the dried samples. The samples were then placed inside a container with 10 mm of water, and they were resting on insulating supports so that the lower face of the prism, not covered by the sealant, was in direct contact with the water. The weight change was measured after 10 min, 90 min to calculate the capillary absorption coefficient C_a [(kg/m^2) $min^{0.5}$] based on Equation (2):

$$C_a = 0.1 \, (M_2 - M_1). \tag{2}$$

For rehabilitation mortars, which should have a low capillary rise value, the weight after 24 h of immersion is also considered, this time measuring C_b [kg/m^2] using Formula (3):

$$C_b = 0.625 \, (M_3 - M_0), \tag{3}$$

being:

M_0: mass in grams when the specimen is dry;
M_1: mass in grams after 10 min of imbibition of the sample;
M_2: mass in grams after 90 min of imbibition of the sample;
M_3: mass in grams after 24 h of imbibition of the sample.

2.3. Chemical Attacks

To understand the chemical durability, the samples were placed in contact with different aggressive environments.

A calcium chloride resistance test was carried out following UNI EN 998-2 [18].

The samples were placed in a 30%wt solution of calcium chloride for 28 days at a temperature of 38 °C to promote the entry of calcium chloride into the matrix, and then at 4 °C for 42 days to promote the formation of calcium oxychloride hydrate. To evaluate the damages of the sample, a compression test on the residual samples was carried out; the tests were performed following the UNI EN 196-1:2005 [19] and using an INSTRON 5567, (INSTRON, Norwood, MA, USA) equipped with a maximum load cell of 30 kN.

Sodium sulfate resistance test was carried out following EN 998-2 [18]. The samples were immersed for 1/3 of their length in a 3.5%wt solution of sodium sulfate for 60 days, monitoring the progress of efflorescence formation.

Finally, in order to evaluate if the presence of earth instead of cement has a beneficial effect within an acidic environment, the samples were placed in contact with 2.15 N hydrochloric acid, 2.15 N nitric acid, and 2.15 N sulfuric acid. The acid concentration is expressed in Normality in order to have the same concentration for monoprotic and biprotic acids. The normality of 2.15 corresponds to 10 wt%, typical for a durability test in cementitious materials. The samples were placed in a beaker with a ratio of acid volume/sample surface area close to 1/8, (about 50 mL of acid). After 7 days the sample has been extracted, dried, and weighed to calculate the weight loss.

2.4. SEM Analysis

To deepen the analysis related to the resistance of materials to chlorides, sulfates, and acids, a microstructural analysis was performed. In the course of the present work,

an ESEM-Quanta 200 scanning electron microscope coupled with EDS analysis (model ESEM-Quanta 200 FEI, coupled with an X-ray EDS microanalysis system, Oxford INCA-350 (Oxford Instruments plc, UK, Tubney Woods, Abingdon, Oxfordshire, UK) was used. Before SEM analysis the sample was coated with an Au-Pd sputtered layer to make the sample conductive.

After chemical attacks SEM analysis was performed on the residual samples to evaluate microstructural modifications and phase formation.

2.5. XRD Analysis

To distinguish the characteristic mineralogic phases of cements with SEs, and especially to see if and how they change after any attack, mineralogical analysis is performed by X-ray powder diffraction.

This test was performed by a powder diffractometer (PW 3710, Philips Research Laboratories, Eindhoven, The Netherlands) with Cu Kα radiation in the 5–70° 2θ range and speed of 1°/min, operating at 40 mA and 40 keV on powdered samples characterized by a grain size of 20–30 μm. Centre for Diffraction Data (ICCD) cards were used to identify the crystalline phases with the aid of XPert High Score Plus software (v3, Malvern Panalytical Ltd., Malvern, Grovewood Road, Malvern, Worcestershire, UK).

3. Results

3.1. True Density, Bulk Density and Porosity

For the physical characterization the results obtained are summarized in Table 3. Looking at the value of bulk density, also defined as specific weight, it is possible to classify SE concrete as a lightweight concrete, having a specific weight of 1.87 i.e., between 0.8 g/cm^3 and 2 g/cm^3, following UNI-EN 206-1:2006 [20]. Lightweight concretes can be used as structural or non-structural, depending on their mechanical properties. This value is comparable to the one reported by Danillo Wisky Silva [21]. The true density of SE sample presents a lower value than OPC (around 3 g/cm^3 as reported by Sadrmomtazi et al.) due to the low cement content in the mixture of this sample [22]. The significant difference between true and bulk density confirms the presence of porosity in the material similar to that of OPC [21].

Table 3. Bulk density, true density, and porosity of the samples (SE = shot-earth; C = concrete; M = mortar).

Sample	V (cm^3)	M (g)	D$_{bulk}$ (g/cm^3)	D$_{true}$ (g/cm^3)	Porosity (%)
SE	59.25	110.84	1.87	2.64	29.03
C	35.00	67.90	1.94	2.68	27.55
M	254.72	465.15	1.83	2.73	33.07

Comparing the results obtained on SE with those for the other types of materials chosen as references, it can be seen that the values are consistent with each other. Especially the values of density and porosity of SE are more similar to those of concrete than to mortar and all of them can be defined as lightweight cements.

3.2. Capillarity Water Absorption

The data obtained from the capillarity absorption are represented in Figure 3.

The uptake trend of SE samples is consistent with that of other samples. All the samples are below 10%, but more similar behavior is shown by SE and C in line with the more similar porosity values. On the contrary the mortar sample shows lower absorption notwithstanding it presents the higher value of porosity. This is probably due to high % of closed porosity and not open porosity in this sample.
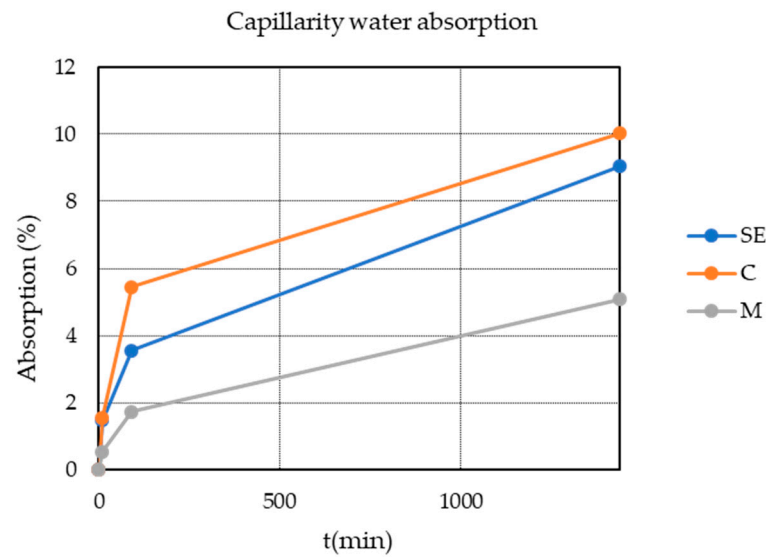
Figure 3. Capillarity water absorption.

Making reference to UNI EN 998-1:2010 [23] regulation, it is possible to include the samples in the categories of water absorption by capillarity. According to Table 4, SE and C samples are included in W1 category, with 0.2 (kg/m^3) min$^{0.5}$ $< C_a <$ 0.4 (kg/m^3) min$^{0.5}$, while M belongs to the W2 category with $C_a <$ 0.2 (kg/m^3) min$^{0.5}$.

Table 4. Categories of capillarity water absorption according to UNI EN 998-1:2010.

W0	W1	W2
$C_a > 0.4$ (kg/m^3) min$^{0.5}$	0.2 (kg/m^3) min$^{0.5}$ $< C_a < 0.4$ (kg/m^3) min$^{0.5}$	$C_a < 0.2$ (kg/m^3) min$^{0.5}$

From the results shown in Figure 4, it is evident that the SE sample is totally consistent with the other samples analyzed and, in some cases, better.
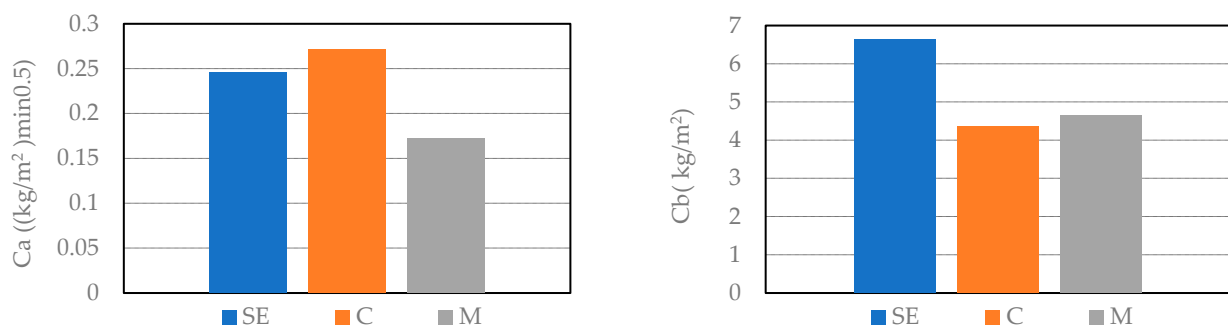

Figure 4. Capillarity absorption coefficients (SE = shot-earth, C = concrete, M = mortar).

Comparing the results obtained in this test with a porosity test (Table 3), we can see that as porosity increases, capillary absorption decreases. This behavior can give us an idea about the type of porosity. In fact, the C samples, while having a lower total porosity than the M samples, absorb more water, which means that their pores are mostly open while those of the M samples are close pores. SE samples are in the middle, so we can say that its open porosity is lower than C samples but higher than M samples. Conversely, SE samples are more sensitive than C and M samples with respect to long term water absorption as measured through the Cb coefficient. This can be ascribed to the presence of micropores in the soil phase of SE samples, through which water penetrates very slowly. This effect

especially occurs in loamy soils. This suggests avoiding the use of SE to realize elements directly exposed to rain, unless proper additives like hydrophobizing agents are added.

3.3. Chemical Attacks

The image of the samples after the calcium chloride resistance test (Figure 5) are the following.
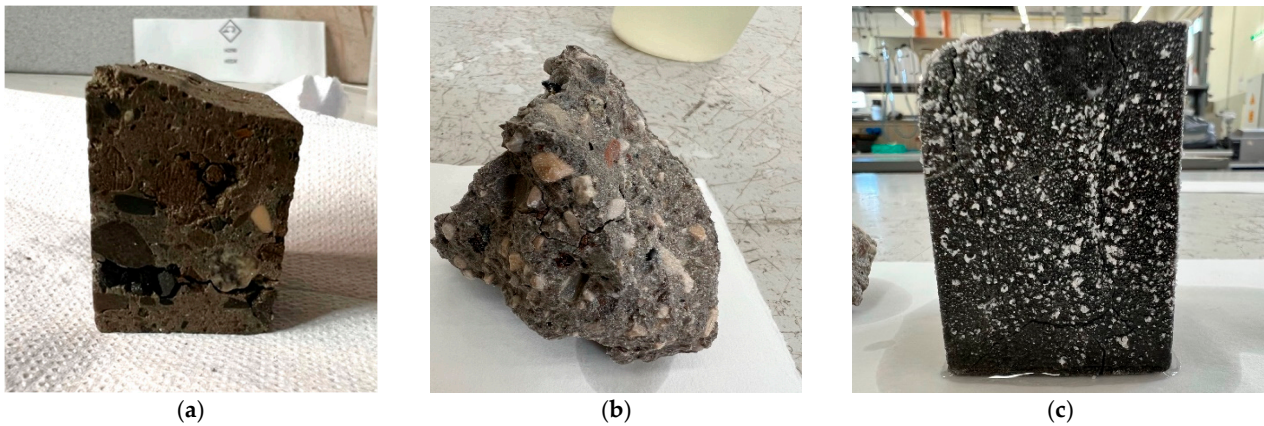

| (**a**) | (**b**) | (**c**) |

Figure 5. SE (**a**), C (**b**) and M (**c**) samples after calcium chloride resistance test.

Figure 5 shows that for the mortar sample (M) the presence of white dots corresponding to Cl salt precipitation is absent in the other two samples. This can be correlated to the calcium chloride attacks on the M sample because it is constituted of cement paste and sand only, while the concrete and the SE also have big aggregates inside them which, since they do not react with calcium chloride, make its action less dangerous. The presence of chlorine in the samples after a chemical attack is also confirmed below by SEM analysis.

The mechanical compression test was then carried out on six samples pre and post attack by calcium chloride.

In the case of M samples, despite the load applied, there is no decrease in compressive strength remaining in the M20 strength class; this may be due to a very high starting strength where the sample does not reach fracture (Figure 6).
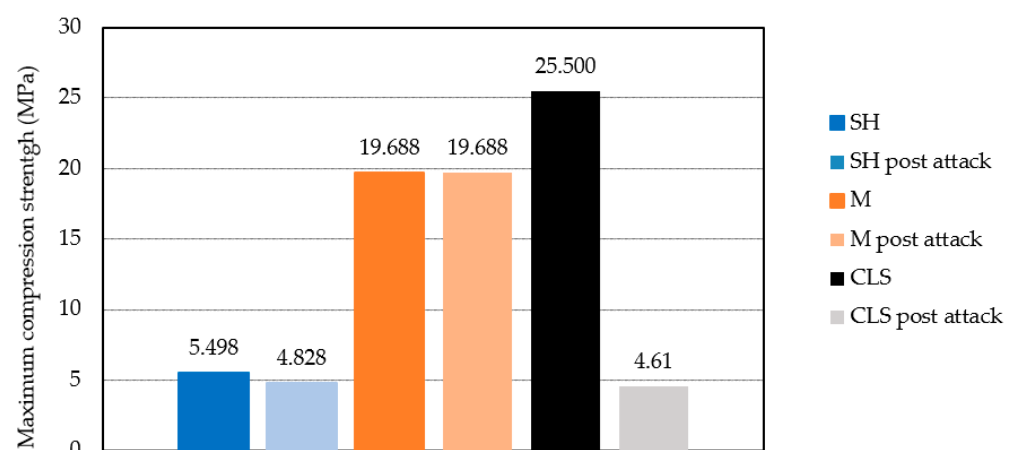

Figure 6. Maximum compressive strength before and after calcium chloride resistance test.

The SE samples have a decrease of about 12% of the maximum compressive strength, but the results are quite satisfied because the samples are still within a good strength class according to UNI EN 998-2 regulation [18], going from a M5 before the test to a M2.5 strength class after the test.

It is worth noticing that the ultimate compressive strength of the concrete samples deeply decreases, going from 25.5 MPa before attack to 4.61 MPa after attack. This can be ascribed to the capacity of $CaCl_2$ to dissolve the cement paste around the aggregates according to the following reaction:

$$3CaCl_2 + Ca(OH)_2 + 14H_2O > 3CaO \cdot CaCl_2 \cdot 15H_2O$$
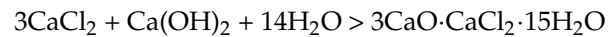
Calcium chloride inside the concrete reacts with $Ca(OH)_2$, formed during the cement hydration, leading to the formation of $3CaO \cdot CaCl_2 \cdot 15H_2O$, which is responsible of the significant mechanical property decrease.

The smaller amount of cement gel in the SE sample leads to the maintenance of the properties due to the lower chemical reactivity.

The other salt used for chemical attack was sodium sulfate, and in Figure 7 the samples after the test are reported.
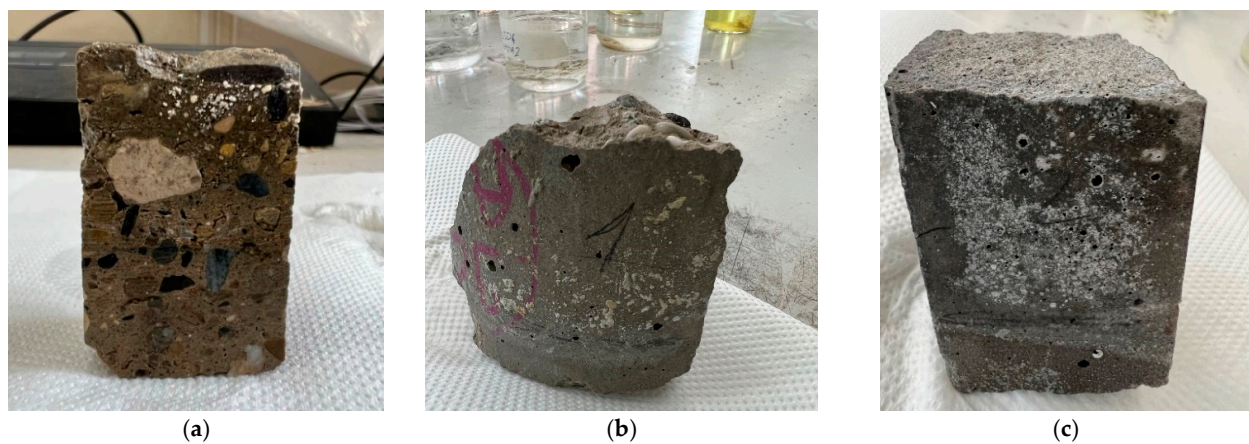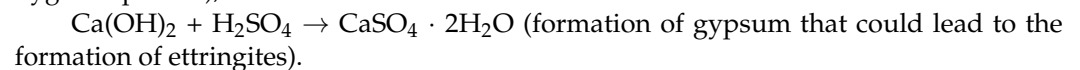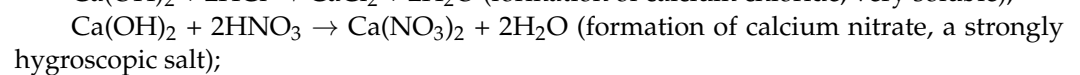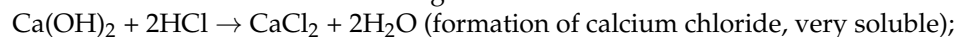

| (a) | (b) | (c) |

Figure 7. SE (**a**), C (**b**) and M (**c**) samples after sodium sulfate resistance test.

There are some small salt crystals formed at the top of the SE samples, but it is evident that these crystals are few and do not seem to have created any major cracks or fractures in the samples, indicating that the presence of gypsum in the SE samples is not much.

In the C sample, whitish formations are noted along the outer surface although not such as to cause obvious damage. In the M sample the walls show white spots. In any case, no structural problems seem to have arisen.

Regarding the acid resistance tests mentioned in Section 2, the reactions that occur within cement materials are the following:

$Ca(OH)_2 + 2HCl \rightarrow CaCl_2 + 2H_2O$ (formation of calcium chloride, very soluble);

$Ca(OH)_2 + 2HNO_3 \rightarrow Ca(NO_3)_2 + 2H_2O$ (formation of calcium nitrate, a strongly hygroscopic salt);

$Ca(OH)_2 + H_2SO_4 \rightarrow CaSO_4 \cdot 2H_2O$ (formation of gypsum that could lead to the formation of ettringites).

The alkaline nature of cement and concrete makes these materials susceptible to acids attacks that are both strong (HCl, HNO_3, H_2SO_4) and weak (CH_3COOH), provoking their decalcification with the loss of soluble calcium salts and the transformation of hydrated silicates into progressively less binding products.

The hydrochloric acid environment is deleterious and the physical–chemical transformations that take place lead to expansive processes that cause the material to break. Türkel et al. [24] observed that the leakage of soluble salts causes an increase in the number and size of the pores of the cement paste as well as accelerating the reaction rate. According to the Chandra twofold model [25] the soluble $CaCl_2$ formed reacts with C_3A phase forming Friedel's salt, $C_3A \cdot CaCl_2 \cdot 10H_2O$, and the interaction between hydrogels may also result in

the formation of some Fe-Si, Al-Si, and Ca-Al-Si complexes which appeared to be stable in pH range above 3.5.

The attack of the cementious matrix by nitric acid produces calcium nitrate that is soluble in water and leachable together by gels of hydrated oxides of Si, Al, and Fe that are sparingly soluble and which constitute a corroded layer. Moreover, Pavlik [26] demonstrated that after about a year of exposure of the cement paste to solutions of low concentrations, an additional zone in the apparently uncorroded core formed containing an increased content of S03.

The most negative effect on cementitious materials is given by sulfuric acid due to the synergistic effect of acid attacks and sulphates [27–29]. By the reaction among calcium aluminates (C_3A) and portlandite (CH) with sulfates ions, two major expansive products are formed: secondary ettringite ($Ca_6Al_2(SO_4)3(OH)12.26H_2O$, a principal destructive compound) and secondary gypsum ($CaSO_4.2H_2O$, soft non-binder compound) [30–32].

The results obtained after the different acid attacks are reported within Figure 8. The weight loss (ΔP%) has been calculated 24 h after taking off the samples from the acid.
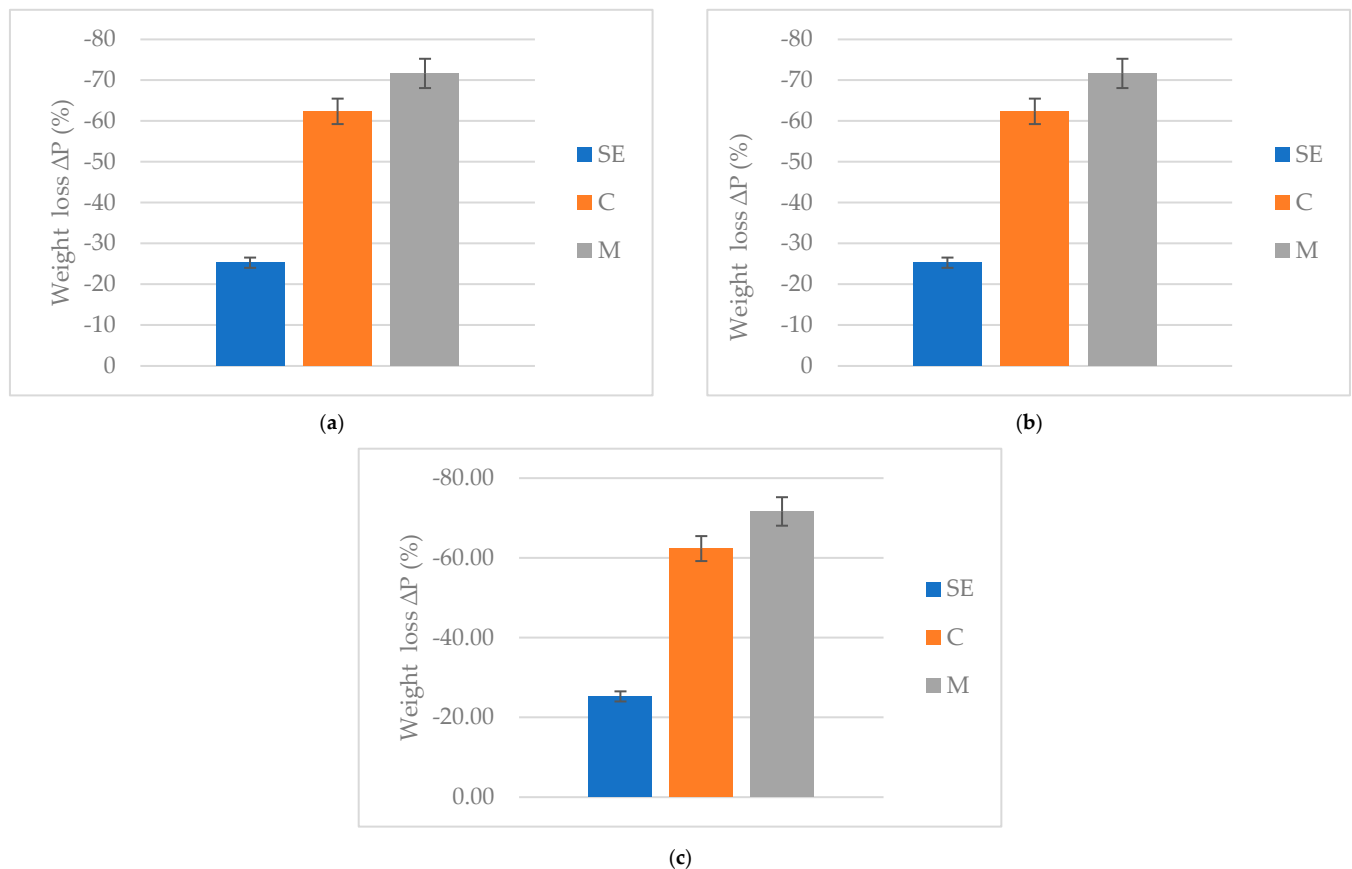

Figure 8. Weight loss % after hydrochloric acid (**a**), nitric acid (**b**), and sulfuric acid (**c**) attack (dust and sample).

Interestingly, hydrochloric acid, which is known to dissolve cement by transforming hydrated lime into calcium chloride, which is very soluble, has less effect in SE samples. This behavior is due to the presence of soil instead of cement, soil being richer in clays and with less lime present, so the material is less susceptible to this type of attack.

In this case also, SE samples perform the best, showing a lower weight loss than other samples. The reason is the same as that reported for hydrochloric acid, namely a lower presence of lime due to replacement of cement by soil, which does not react and gives the sample less reactivity with this type of acid.

Both nitric and hydrochloric acids also decompose the silicates and aluminates present in the cement matrix, thus confirming the fact that SE samples are more resistant to these acids since they contain less cement.

On the contrary, in the case of sulfuric acid the weight loss varies greatly if one considers the residual dust or not, and this means that the samples have been disintegrated but most of the powder formed is not dissolved in the solution. Sulfuric acid, when in contact with lime, forms gypsum; the formation of gypsum means that the weight loss is not as noticeable because the chemical nature of some elements has changed but these elements have not been dissolved in the acid.

3.4. SEM Analyses

SEM analyses were first performed on the pre attack SE samples, and the images obtained are reported in Figure 9.
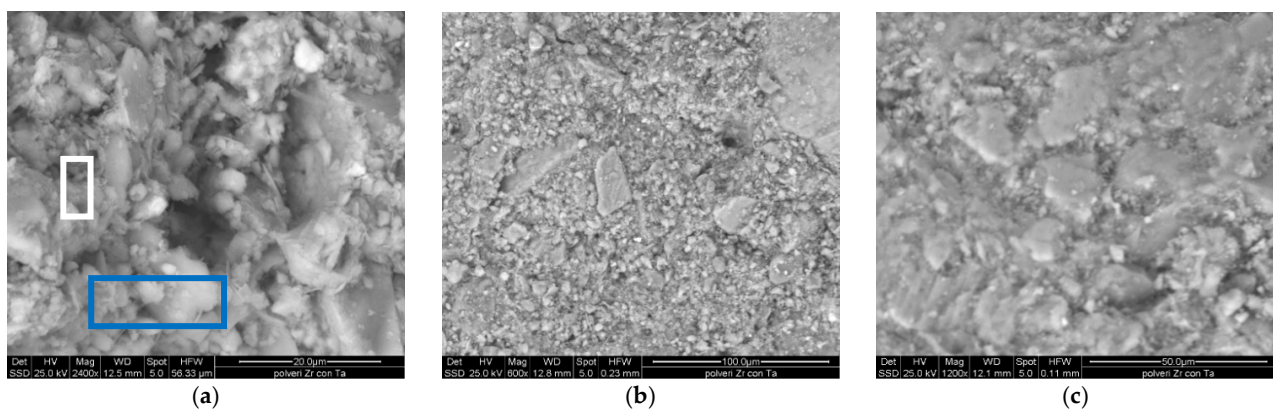

Figure 9. SEM images of pre attached SE samples. (**a**) (600×). (**b**) (1200×). (**c**) (2400×) Blue rectangles = gel area, White rectangle = aggregate.

The earth and cement fractions are well blended together as the binder matrix appears homogeneous. Some aggregates with dimensions between 10 and 20 μm are also distinguishable, and the interface between aggregate and matrix presents good adhesion.

In Figure 9a it is possible to see two highlighted areas. The blue area corresponds to cementitious gel with a chemical composition corresponding to Si = 20 wt% and Ca = 30%, determined by EDS analysis. The chemical composition of the aggregate (white area) shows a higher amount of silicon and a lower amount of Ca (Si = 28% and Ca = 7%), in agreement with siliceous aggregates. In the interface area intermediate chemical composition is observed, i.e. Si = 20% and Ca = 26% due to the chemical interaction between matrix and aggregate. The presence of the mentioned elements is shown in the EDS graphic of the blue area of the sample. In the post chloride attack of SE specimens, both inner and outer surfaces were analyzed, and the images are reported in Figure 10.

The samples appear to be fairly homogeneous both internally and externally, and no diffuse salt precipitation is observed. The main elements found in the examined samples are Silicon, Calcium, Aluminum, Magnesium, Chlorine, Iron, and Sodium. On the sample surface, the presence of chlorine is significant (about 6%), considering that it is only due to eluate residues, probably deposit is formed. Only in the outer surface samples, rare white dots are evident, with a chemical composition of Ca = 20% and Cl = 5%, corresponding to crystallization of calcium chlorides.

The chemical analysis of aggregate particles remains unchanged, corresponding to Si and O in agreement with their siliceous natures. From the chemical analysis of the inner part of the samples a significant concentration of chlorine is observed in the cementitious gel (Cl = 3.7–9wt%). From these data it seems that chlorine diffuses in the gel more than it concentrates in the crystals.
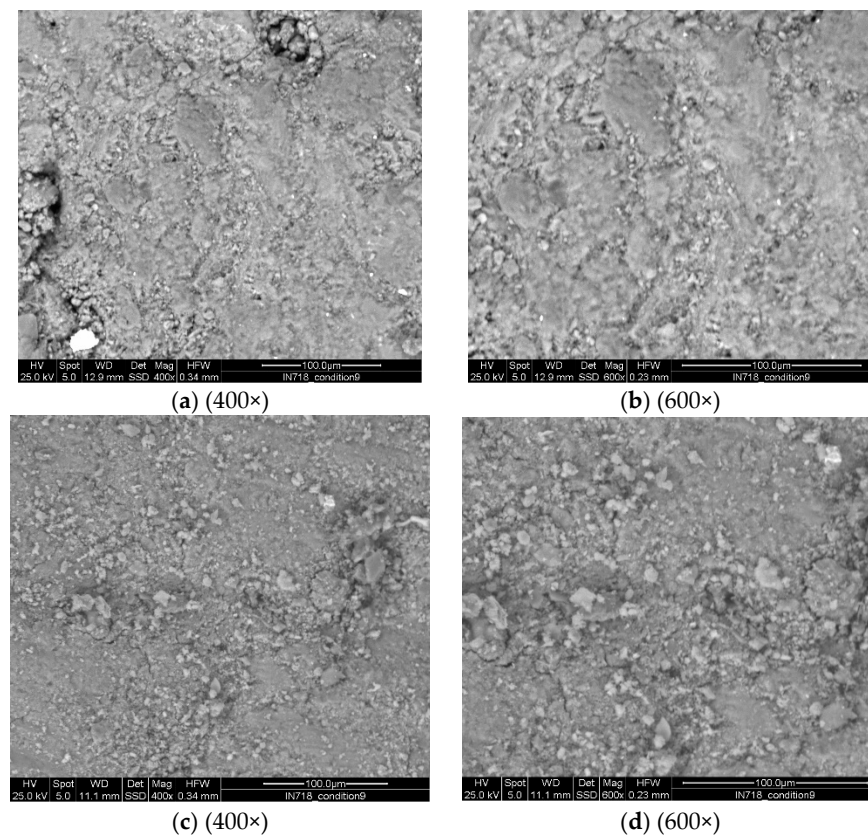
Figure 10. SEM images of outer surfaces (**a**,**b**) and inner (**c**,**d**) in SE sample post calcium chloride attack.

The presence of the Cl on the sample surface is also confirmed by the chemical analysis reported in Figure 11.
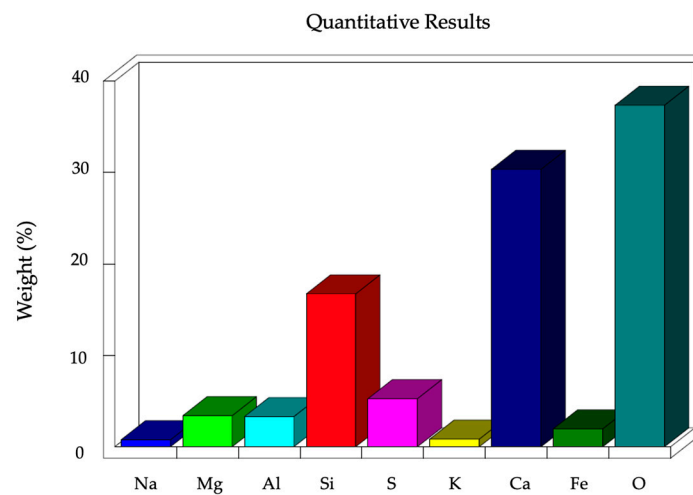

Figure 11. Semiquantitative chemical analysis of the outer surface of the SE sample after calcium chloride attack.

Regarding post attack samples from sodium sulfate, SEM images were taken from both the samples from the emerged side (thus where ettringite eventually forms, Figure 12a) and the immersed side (Figure 12b) and compared with the pre attack SE samples (Figure 9).
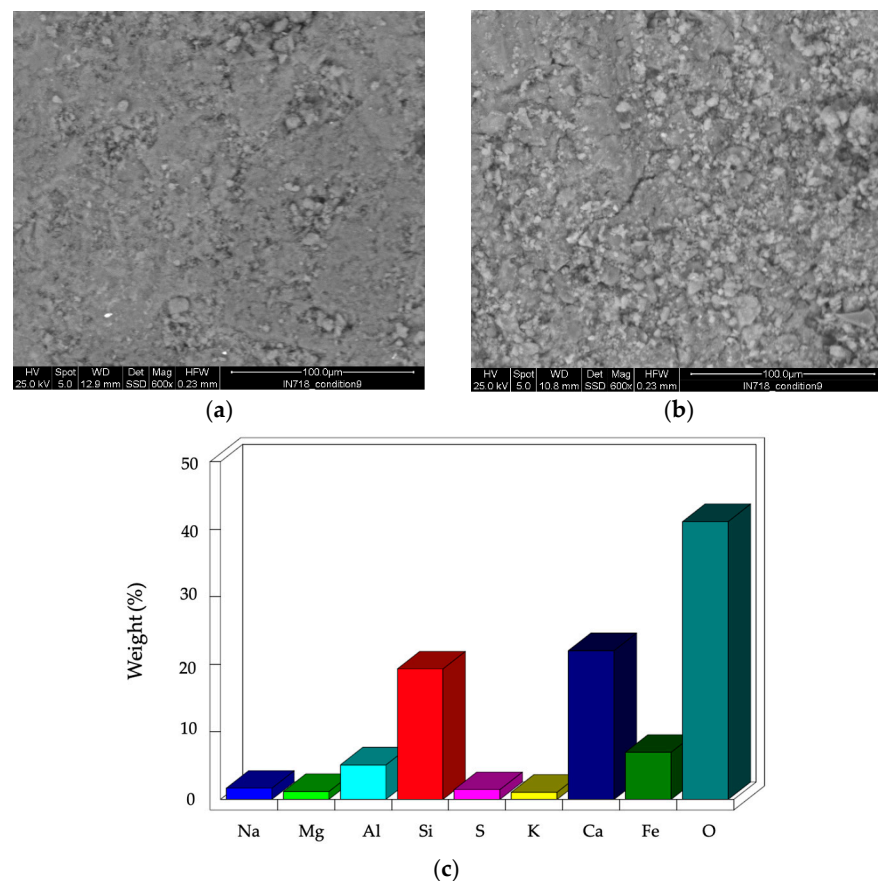
Figure 12. SEM images of the SE sample post sodium sulfate ((**a**) (600×)) emerged part and ((**b**) (600×)) immersed part. (**c**) Semiquantitative chemical analysis of emerged part.

It is worth noticing that no salts or fractures are evident from the images and the matrix appears to be homogeneous.

The elements present in the SE samples are mainly Calcium, Magnesium, Iron, Aluminum, Potassium, and Silicon (Figure 12). The percentages of these elements vary slightly, probably depending on the concentration of soil or the presence of aggregates, but since the soil and cement are perfectly amalgamated, it is impossible to state which elements relate to the soil alone and which to the cement.

Analyzing the immersed part makes it evident that Sulphur is homogenously distributed in the sample with a concentration of 1.1–1.95%, but it is particularly concentrated in the cementitious gel with an average concentration of 4 wt% (Figure 12).

Also, analysis of the sample corresponding to the surface content of Sulphur that is not immersed is also observed, and this probably can be related to diffusion of Sulphur inside the sample.

3.5. XRD Analyses

XRD analysis was carried out, for all types of samples, pre attack, after acid attack, after calcium chloride attack, and after sodium sulfate attack, to see the crystal structure of the samples and whether this changes after exposure to aggressive agents.

Comparisons were then made to see how the crystal structure changed in the different situations, i.e., in contact with calcium chloride and hydrochloric acid, sodium sulfate and sulfuric acid, and finally in contact with nitric acid.

- HCl and calcium chloride

The crystalline phases present in the SE pre attack samples are quartz coming from both aggregates, matrix, and calcite. After an attack by calcium chloride, a slight decrease in the peak related to calcite (29°) is seen, but the graphs remain about the same. After the attack by hydrochloric acid, on the other hand, the peak relating to calcite (29°) disappears, due to the high solubility of this phase in HCl, and quartz remains the only phase present (Figure 13a). This is because the calcium present in the form of calcium hydroxide reacts with hydrochloric acid to form calcium chloride, which is a very soluble substance, so only the quartz of the aggregates remains in the sample, which does not dissolve in contact with the acid.

In pre attack concrete and mortar (Figure 13b,c) samples, in addition to quartz and calcite, dolomite is also present. In both samples after attack by calcium chloride (Figure 13b,c), the peaks of the dolomite and calcite decrease in favor of quartz, although the crystalline phases do not change. After the attack of hydrochloric acid, the peaks for calcite and dolomite disappear in favor of a quartz increase, since calcium has reacted and turned into calcium chloride.

- H_2SO_4 and sodium sulfate

The pre and post attack XRD patterns from sodium sulfate appears to be quite similar for every sample, and only few small peaks related to calcite decrease for SE (Figure 14a), while for C (Figure 14b) and M (Figure 14c) samples the dolomite peak decreases significantly in favor of calcite.

On the contrary, with the acid attack, XRD patterns pre and post acid attack change significantly; calcium in the form of calcium hydroxide in contact with sulfuric acid forms gypsum, which in the case of the SE sample is present in an important way (peaks at 11°, 21°, 29°, 31°, 33°), going on to consume all the calcite whose peaks disappear. The peaks related to quartz, on the other hand, remain almost unchanged, since quartz does not react with the acid. Gypsum, quartz, and residual calcite or dolomite are the crystalline phases present post sulfuric acid attack.

- HNO_3

For nitric acid there is no comparison with the related salt, but it is interesting to see how the peaks related to calcite (and for the C and M samples also to dolomite) disappear due to their solubility and the free Ca formed reacts with the acid to form calcium nitrate. Quartz remains the only crystalline phase present after a nitric acid attack for all the samples (Figure 15).

In general, what can be said in relation to all the XRD patterns examined is that the samples behave consistently with each other, and those containing more aggregates (and therefore more quartz) are more resistant to attacks, especially acid attacks. SE samples turn out to be more resistant to attacks because, in addition to containing aggregates, they contain less calcium since part of the cement is replaced by soil, and this allows for less reactivity and consequently leads to a lower weight loss. These considerations are consistent for all the salts and the acids tested, except for nitric acid, where the weight loss turns out to be greater for SE than in the other samples tested.
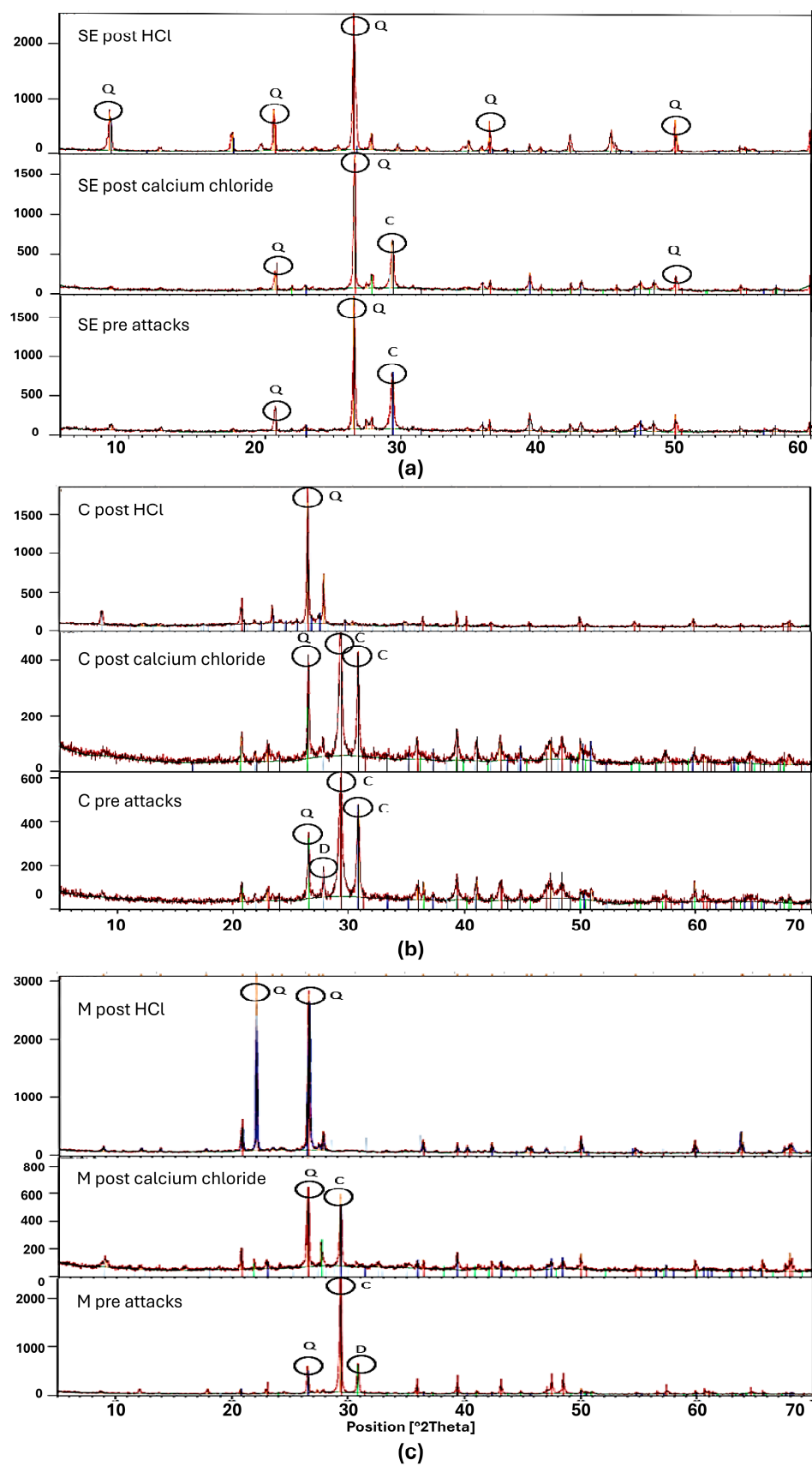
Figure 13. SE (**a**), C (**b**), and M (**c**) comparison pre attack, after calcium chloride, and post hydrochloric acid attack. (C = calcite, Q = quartz, D = dolomite).
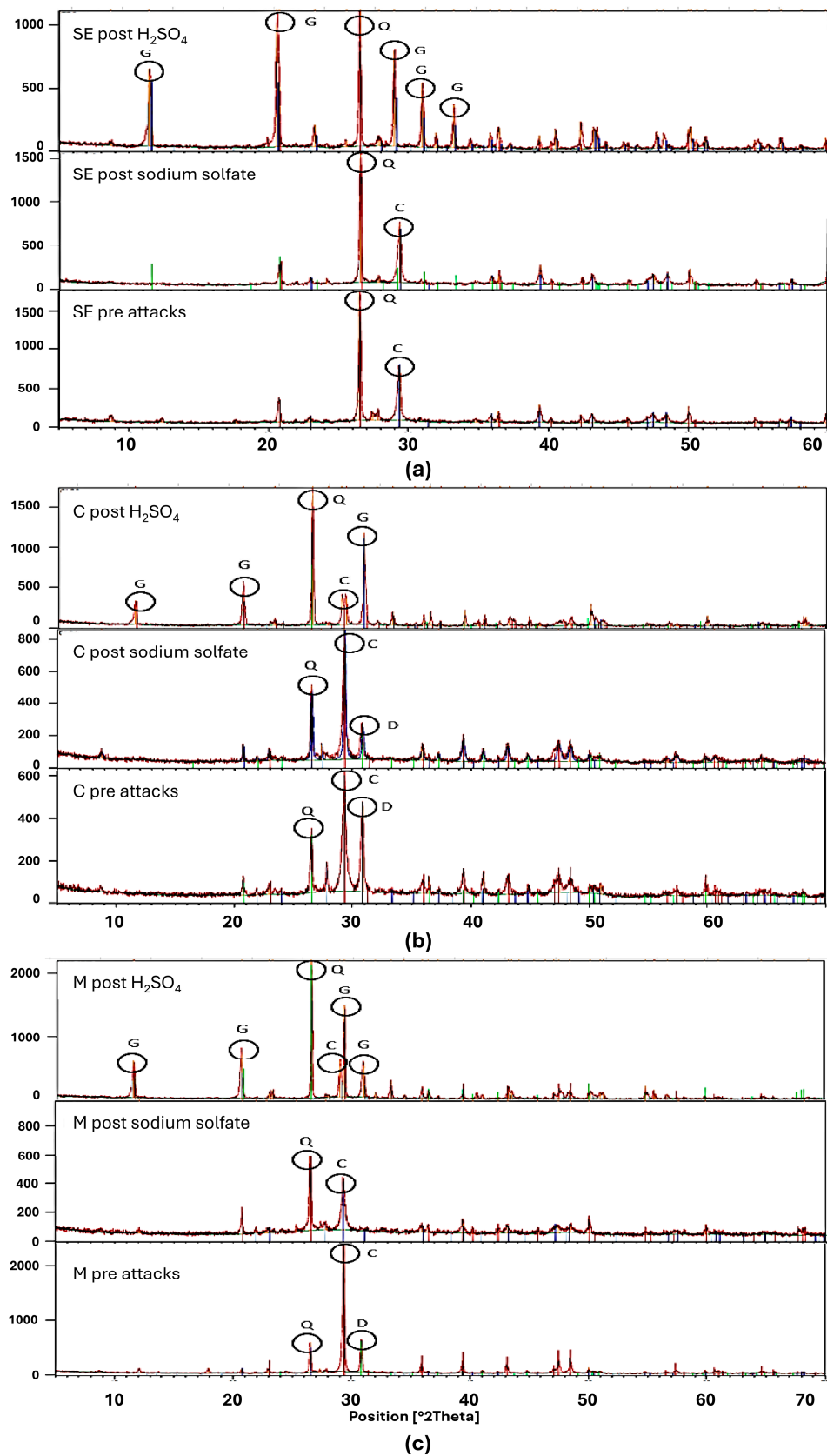
Figure 14. SE (**a**), C (**b**), and M (**c**) comparison pre attack, post sodium sulfate, and post sulfuric acid attack. (C = calcite, Q = quartz, D = dolomite, G = Gypsum).
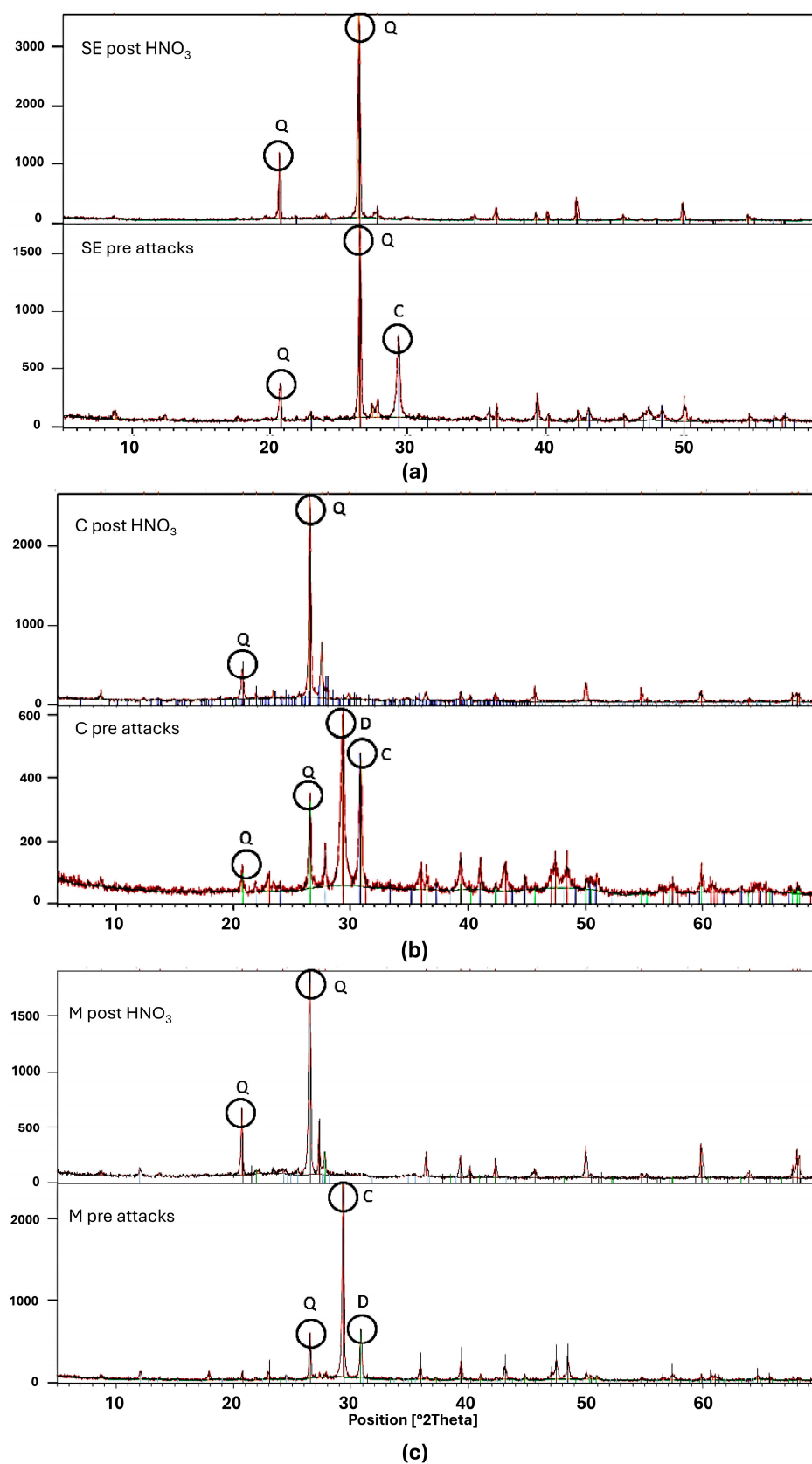
Figure 15. SE (**a**), C (**b**), and M (**c**) comparison before and after nitric acid attack. (C = calcite, Q = quartz, D = dolomite).

4. Conclusions

The main physical and chemical performances of SE samples have been identified through a comprehensive experimental campaign and compared to those exhibited by conventional cementitious composites like concrete and mortar. Summing up, this study carried out yields with positive implications. In detail, the values of the true density (2636 g/cm^3) and porosity (29%) confirm that the SE samples are in line with the reference ones. The same can be said for the capillary water absorption test, which places the SE samples in category W1 according to UNI EN 998-1:2010, the same category as mortar. Although mechanically weaker, SE specimens are generally more resistant to chemical attack by salts, precisely because of the presence of earth that replaces cement and does not react. The compressive strength remains almost constant after chemical attack, while for concrete, a dramatic decrease in this property is evident (25.5 MPa before and 4.6 MPa after the CaC_{l2} attack).

Even in acid attacks, the substitution of cement by earth plays an important role in the resistance of the samples to acid contact. In particular, the SE samples also showed greater resistance to nitric acid and hydrochloric acid than the reference samples, reporting a lower percentage of weight loss, 25% for hydrochloric acid and 45% for nitric acid. This is because the soil used in SE samples replaces part of the cement, resulting in less lime available to react. However, with sulfuric acid, there is a greater weight loss from SE samples compared to the reference ones, although it is still a relatively low value (21%). These results have been corroborated by XRD and SEM analyses, which allow for assessing the final conditions of the samples after acid attacks. The investigation confirms that the SE samples have good resistance to chemical attacks.

Therefore, given the results obtained in this study, it is possible to conclude that the durability of SE samples is perfectly in line with that of mortar and concrete, if not, in some cases, even better. The outcomes obtained in the present paper can be interpreted as a benchmark to corroborate further investigations about the durability of SE construction. Particularly, this study highlighted that the durability of SE and soil-based material must be assessed, taking into account specific chemical and physical aspects to avoid implementing durability-enhancing strategies at the mix design or technological level that are not needed nor effective. Finally, this study will permit the creation of further optimization strategies for construction in sustainable excavated soil leading to the use of less cement with a corresponding lower amount of CO_2 emitted for the clinker production.

References

1. Hale, S.E.; Roque, A.J.; Okkenhaug, G.; Sørmo, E.; Lenoir, T.; Carlsson, C.; Kupryianchyk, D.; Flyhammar, P.; Žlender, B. The Reuse of Excavated Soils from Construction and Demolition Projects: Limitations and Possibilities. *Sustainability* **2021**, *13*, 6083. [CrossRef]
2. Tarantino, A.M.; Cotana, F.; Viviani, M. (Eds.) *Shot-Earth for an Eco-Friendly and Human-Comfortable Construction Industry*; Springer Tracts in Civil Engineering; Springer Nature: Cham, Switzerland, 2023; ISBN 978-3-031-23506-1.
3. Savino, V.; Franciosi, M.; Viviani, M. Engineering and Analyses of a Novel Catalan Vault. *Eng. Fail. Anal.* **2023**, *143*, 106841. [CrossRef]
4. Scrivener, K.; Martirena, F.; Bishnoi, S.; Maity, S. Calcined Clay Limestone Cements (LC3). *Cem. Concr. Res.* **2018**, *114*, 49–56. [CrossRef]
5. Bacciocchi, M.; Savino, V.; Lanzoni, L.; Tarantino, A.M.; Viviani, M. Multi-Phase Homogenization Procedure for Estimating the Mechanical Properties of Shot-Earth Materials. *Compos. Struct.* **2022**, *295*, 115799. [CrossRef]
6. Curto, A.; Lanzoni, L.; Tarantino, A.M.; Viviani, M. Shot-Earth for Sustainable Constructions. *Constr. Build. Mater.* **2020**, *239*, 117775. [CrossRef]
7. D'Alessandro, A.; Fabiani, C.; Pisello, A.L.; Ubertini, F.; Materazzi, A.L.; Cotana, F. Innovative Concretes for Low-Carbon Constructions: A Review. *Int. J. Low-Carbon Tech.* **2016**, *12*, 289–309. [CrossRef]
8. Elsvier Article: Shot-Earth for Sustainable Constructions. Available online: https://www.pittet-artisans.ch/blog/elsvier-article-shot-earth-for-sustainable-constructions.html (accessed on 12 January 2020).
9. Robalo, K.; Soldado, E.; Costa, H.; Carvalho, L.; Do Carmo, R.; Júlio, E. Durability and Time-Dependent Properties of Low-Cement Concrete. *Materials* **2020**, *13*, 3583. [CrossRef] [PubMed]
10. Soldado, E.; Antunes, A.; Costa, H.; Do Carmo, R.; Júlio, E. Durability of Mortar Matrices of Low-Cement Concrete with Specific Additions. *Constr. Build. Mater.* **2021**, *309*, 125060. [CrossRef]
11. Scherer, G.W. Stress from Crystallization of Salt. *Cem. Concr. Res.* **2004**, *34*, 1613–1624. [CrossRef]
12. Medina, G.; Sáez Del Bosque, I.F.; Frías, M.; Sánchez De Rojas, M.I.; Medina, C. Durability of New Recycled Granite Quarry Dust-Bearing Cements. *Constr. Build. Mater.* **2018**, *187*, 414–425. [CrossRef]
13. Tobón, J.I.; Payá, J.; Restrepo, O.J. Study of Durability of Portland Cement Mortars Blended with Silica Nanoparticles. *Constr. Build. Mater.* **2015**, *80*, 92–97. [CrossRef]
14. Vantadori, S.; Żak, A.; Sadowski, Ł.; Ronchei, C.; Scorza, D.; Zanichelli, A.; Viviani, M. Microstructural, Chemical and Physical Characterisation of the Shot-Earth 772. *Constr. Build. Mater.* **2022**, *341*, 127766. [CrossRef]
15. Colpo, A.; Vantadori, S.; Friedrich, L.; Zanichelli, A.; Ronchei, C.; Scorza, D.; Iturrioz, I. A Novel LDEM Formulation with Crack Frictional Sliding to Estimate Fracture and Flexural Behaviour of the Shot-Earth 772. *Compos. Struct.* **2023**, *305*, 116514. [CrossRef]
16. *UNI EN 1936:2006*; Test Methods for Natural Stones—Determination of Real and Apparent Density and Total and Open Porosity. UNI: Rome, Italy, 2006.
17. *UNI EN 1015-18:2004*; Test Methods for Masonry Mortars—Determination of the Capillarity Water Absorption Coefficient of the Hardened Mortar. UNI: Rome, Italy, 2004.
18. *UNI EN 998-2:2016*; Specifications for Masonry Mortars—Part 2: Masonry Mortars. UNI: Rome, Italy, 2016.
19. *EN 196-1:2005*; Methods of Testing Cement—Part 1: Determination of Strength. UNI: Rome, Italy, 2005.
20. *UNI-EN 206-1:2006*; Concrete—Part 1: Specification, Performance, Production and Conformity. UNI: Rome, Italy, 2006.
21. Danillo Wisky Silva, L.; Bufalino, M.A.; Martins, H.S.; Junior, G.; Tonoli, L. Mendes, Superabsorbent Ability Polymer to Reduce the Bulk Density of Extruded Cement Boards. *J. Build. Eng.* **2021**, *43*, 103130. [CrossRef]
22. Sadrmomtazi, A.; Noorollahi, Z.; Tahmouresi, B.; Saradar, A. Effects of Hauling Time on Self-Consolidating Mortars Containing Metakaolin and Natural Zeolite. *Constr. Build. Mater.* **2019**, *221*, 283–291. [CrossRef]
23. *UNI EN 998-1:2010*; Specification for mortar for masonry—Part 1: Rendering and plastering mortar. UNI: Rome, Italy, 2011.
24. Türkel, S.; Felekoğlu, B.; Dulluç, S. Influence of Various Acids on the Physico-Mechanical Properties of Pozzolanic Cement Mortars. *Sadhana* **2007**, *32*, 683–691. [CrossRef]
25. Chandra, S. Hydrochloric Acid Attack on Cement Mortar—An Analytical Study. *Cem. Concr. Res.* **1988**, *18*, 193–203. [CrossRef]
26. Pavlík, V. Corrosion of Hardened Cement Paste by Acetic and Nitric Acids Part II: Formation and Chemical Composition of the Corrosion Products Layer. *Cem. Concr. Res.* **1994**, *24*, 1495–1508. [CrossRef]
27. Sahoo, S.; Das, B.B.; Mustakim, S. Acid, Alkali, and Chloride Resistance of Concrete Composed of Low-Carbonated Fly Ash. *J. Mater. Civ. Eng.* **2017**, *29*, 04016242. [CrossRef]
28. Min, H.; Song, Z. Investigation on the Sulfuric Acid Corrosion Mechanism for Concrete in Soaking Environment. *Adv. Mater. Sci. Eng.* **2018**, *2018*, 3258123. [CrossRef]
29. Irico, S.; De Meyst, L.; Qvaeschning, D.; Alonso, M.C.; Villar, K.; De Belie, N. Severe Sulfuric Acid Attack on Self-Compacting Concrete with Granulometrically Optimized Blast-Furnace Slag-Comparison of Different Test Methods. *Materials* **2020**, *13*, 1431. [CrossRef] [PubMed]
30. Jankovic, K.; Milicic, L.; Stankovic, S.; SuSic, N. Investigation of the Mortar and Concrete Resistance in Aggressive Solutions. *Teh. Vjesn.* **2014**, *21*, 173–176.

31. Bin, T.; Cohen, M.D. Does Gypsum Formation during Sulfate Attack on Concrete Lead to Expansion? *Cement Concr. Res.* **2000**, *30*, 117–123.
32. Tian, B.; Cohen, M.D. Expansion of Alite Paste Caused by Gypsum Formation during Sulfate Attack. *J. Mater. Civ. Eng.* **2000**, *12*, 24–25. [CrossRef]